Dalitz plot analysis of $\eta_c \to K^+K^-\eta$ and $\eta_c \to K^+K^-\pi^0$ in two-photon interactions

J. P. Lees,[1] V. Poireau,[1] V. Tisserand,[1] E. Grauges,[2] A. Palano,[3a,3b] G. Eigen,[4] B. Stugu,[4] D. N. Brown,[5] L. T. Kerth,[5] Yu. G. Kolomensky,[5] M. J. Lee,[5] G. Lynch,[5] H. Koch,[6] T. Schroeder,[6] C. Hearty,[7] T. S. Mattison,[7] J. A. McKenna,[7] R. Y. So,[7] A. Khan,[8] V. E. Blinov,[9a,9c] A. R. Buzykaev,[9a] V. P. Druzhinin,[9a,9b] V. B. Golubev,[9a,9b] E. A. Kravchenko,[9a,9b] A. P. Onuchin,[9a,9c] S. I. Serednyakov,[9a,9b] Yu. I. Skovpen,[9a,9b] E. P. Solodov,[9a,9b] K. Yu. Todyshev,[9a,9b] A. J. Lankford,[10] M. Mandelkern,[10] B. Dey,[11] J. W. Gary,[11] O. Long,[11] C. Campagnari,[12] M. Franco Sevilla,[12] T. M. Hong,[12] D. Kovalskyi,[12] J. D. Richman,[12] C. A. West,[12] A. M. Eisner,[13] W. S. Lockman,[13] W. Panduro Vazquez,[13] B. A. Schumm,[13] A. Seiden,[13] D. S. Chao,[14] C. H. Cheng,[14] B. Echenard,[14] K. T. Flood,[14] D. G. Hitlin,[14] T. S. Miyashita,[14] P. Ongmongkolkul,[14] F. C. Porter,[14] R. Andreassen,[15] Z. Huard,[15] B. T. Meadows,[15] B. G. Pushpawela,[15] M. D. Sokoloff,[15] L. Sun,[15] P. C. Bloom,[16] W. T. Ford,[16] A. Gaz,[16] J. G. Smith,[16] S. R. Wagner,[16] R. Ayad,[17,†] W. H. Toki,[17] B. Spaan,[18] D. Bernard,[19] M. Verderi,[19] S. Playfer,[20] D. Bettoni,[21a] C. Bozzi,[21a] R. Calabrese,[21a,21b] G. Cibinetto,[21a,21b] E. Fioravanti,[21a,21b] I. Garzia,[21a,21b] E. Luppi,[21a,21b] L. Piemontese,[21a] V. Santoro,[21a] A. Calcaterra,[22] R. de Sangro,[22] G. Finocchiaro,[22] S. Martellotti,[22] P. Patteri,[22] I. M. Peruzzi,[22,§] M. Piccolo,[22] M. Rama,[22] A. Zallo,[22] R. Contri,[23a,23b] M. Lo Vetere,[23a,23b] M. R. Monge,[23a,23b] S. Passaggio,[23a] C. Patrignani,[23a,23b] E. Robutti,[23a] B. Bhuyan,[24] V. Prasad,[24] M. Morii,[25] A. Adametz,[26] U. Uwer,[26] H. M. Lacker,[27] P. D. Dauncey,[28] U. Mallik,[29] C. Chen,[30] J. Cochran,[30] S. Prell,[30] H. Ahmed,[31] A. V. Gritsan,[32] N. Arnaud,[33] M. Davier,[33] D. Derkach,[33] G. Grosdidier,[33] F. Le Diberder,[33] A. M. Lutz,[33] B. Malaescu,[33,‡] P. Roudeau,[33] A. Stocchi,[33] G. Wormser,[33] D. J. Lange,[34] D. M. Wright,[34] J. P. Coleman,[35] J. R. Fry,[35] E. Gabathuler,[35] D. E. Hutchcroft,[35] D. J. Payne,[35] C. Touramanis,[35] A. J. Bevan,[36] F. Di Lodovico,[36] R. Sacco,[36] G. Cowan,[37] J. Bougher,[38] D. N. Brown,[38] C. L. Davis,[38] A. G. Denig,[39] M. Fritsch,[39] W. Gradl,[39] K. Griessinger,[39] A. Hafner,[39] E. Prencipe,[39] K. R. Schubert,[39] R. J. Barlow,[40,¶] G. D. Lafferty,[40] R. Cenci,[41] B. Hamilton,[41] A. Jawahery,[41] D. A. Roberts,[41] R. Cowan,[42] G. Sciolla,[42] R. Cheaib,[43] P. M. Patel,[43,*] S. H. Robertson,[43] N. Neri,[44a] F. Palombo,[44a,44b] L. Cremaldi,[45] R. Godang,[45,**] P. Sonnek,[45] D. J. Summers,[45] M. Simard,[46] P. Taras,[46] G. De Nardo,[47a,47b] G. Onorato,[47a,47b] C. Sciacca,[47a,47b] M. Martinelli,[48] G. Raven,[48] C. P. Jessop,[49] J. M. LoSecco,[49] K. Honscheid,[50] R. Kass,[50] E. Feltresi,[51a,51b] M. Margoni,[51a,51b] M. Morandin,[51a] M. Posocco,[51a] M. Rotondo,[51a] G. Simi,[51a,51b] F. Simonetto,[51a,51b] R. Stroili,[51a,51b] S. Akar,[52] E. Ben-Haim,[52] M. Bomben,[52] G. R. Bonneaud,[52] H. Briand,[52] G. Calderini,[52] J. Chauveau,[52] Ph. Leruste,[52] G. Marchiori,[52] J. Ocariz,[52] M. Biasini,[53a,53b] E. Manoni,[53a] S. Pacetti,[53a,53b] A. Rossi,[53a] C. Angelini,[54a,54b] G. Batignani,[54a,54b] S. Bettarini,[54a,54b] M. Carpinelli,[54a,54b,††] G. Casarosa,[54a,54b] A. Cervelli,[54a,54b] M. Chrzaszcz,[54a,54b] F. Forti,[54a,54b] M. A. Giorgi,[54a,54b] A. Lusiani,[54a,54c] B. Oberhof,[54a,54b] E. Paoloni,[54a,54b] A. Perez,[54a] G. Rizzo,[54a,54b] J. J. Walsh,[54a] D. Lopes Pegna,[55] J. Olsen,[55] A. J. S. Smith,[55] R. Faccini,[56a,56b] F. Ferrarotto,[56a] F. Ferroni,[56a,56b] M. Gaspero,[56a,56b] L. Li Gioi,[56a] G. Piredda,[56a] C. Bünger,[57] S. Dittrich,[57] O. Grünberg,[57] T. Hartmann,[57] M. Hess,[57] T. Leddig,[57] C. Voß,[57] R. Waldi,[57] T. Adye,[58] E. O. Olaiya,[58] F. F. Wilson,[58] S. Emery,[59] G. Vasseur,[59] F. Anulli,[60,‡‡] D. Aston,[60] D. J. Bard,[60] C. Cartaro,[60] M. R. Convery,[60] J. Dorfan,[60] G. P. Dubois-Felsmann,[60] W. Dunwoodie,[60] M. Ebert,[60] R. C. Field,[60] B. G. Fulsom,[60] M. T. Graham,[60] C. Hast,[60] W. R. Innes,[60] P. Kim,[60] D. W. G. S. Leith,[60] P. Lewis,[60] D. Lindemann,[60] S. Luitz,[60] V. Luth,[60] H. L. Lynch,[60] D. B. MacFarlane,[60] D. R. Muller,[60] H. Neal,[60] M. Perl,[60] T. Pulliam,[60] B. N. Ratcliff,[60] A. Roodman,[60] A. A. Salnikov,[60] R. H. Schindler,[60] A. Snyder,[60] D. Su,[60] M. K. Sullivan,[60] J. Va'vra,[60] A. P. Wagner,[60] W. F. Wang,[60] W. J. Wisniewski,[60] H. W. Wulsin,[60] M. V. Purohit,[61] R. M. White,[61,§§] J. R. Wilson,[61] A. Randle-Conde,[62] S. J. Sekula,[62] M. Bellis,[63] P. R. Burchat,[63] E. M. T. Puccio,[63] M. S. Alam,[64] J. A. Ernst,[64] R. Gorodeisky,[65] N. Guttman,[65] D. R. Peimer,[65] A. Soffer,[65] S. M. Spanier,[66] J. L. Ritchie,[67] A. M. Ruland,[67] R. F. Schwitters,[67] B. C. Wray,[67] J. M. Izen,[68] X. C. Lou,[68] F. Bianchi,[69a,69b] F. De Mori,[69a,69b] A. Filippi,[69a] D. Gamba,[69a,69b] L. Lanceri,[70a,70b] L. Vitale,[70a,70b] F. Martinez-Vidal,[71] A. Oyanguren,[71] P. Villanueva-Perez,[71] J. Albert,[72] Sw. Banerjee,[72] A. Beaulieu,[72] F. U. Bernlochner,[72] H. H. F. Choi,[72] G. J. King,[72] R. Kowalewski,[72] M. J. Lewczuk,[72] T. Lueck,[72] I. M. Nugent,[72] J. M. Roney,[72] R. J. Sobie,[72] N. Tasneem,[72] T. J. Gershon,[73] P. F. Harrison,[73] T. E. Latham,[73] H. R. Band,[74] S. Dasu,[74] Y. Pan,[74] R. Prepost,[74] and S. L. Wu[74]

(The *BABAR* Collaboration)

[1]*Laboratoire d'Annecy-le-Vieux de Physique des Particules (LAPP), Université de Savoie, CNRS/IN2P3, F-74941 Annecy-Le-Vieux, France*
[2]*Universitat de Barcelona, Facultat de Fisica, Departament ECM, E-08028 Barcelona, Spain*
[3a]*INFN Sezione di Bari, I-70126 Bari, Italy*
[3b]*Dipartimento di Fisica, Università di Bari, I-70126 Bari, Italy*
[4]*University of Bergen, Institute of Physics, N-5007 Bergen, Norway*
[5]*Lawrence Berkeley National Laboratory and University of California, Berkeley, California 94720, USA*
[6]*Ruhr Universität Bochum, Institut für Experimentalphysik 1, D-44780 Bochum, Germany*
[7]*University of British Columbia, Vancouver, British Columbia, Canada V6T 1Z1*

[8]*Brunel University, Uxbridge, Middlesex UB8 3PH, United Kingdom*
[9a]*Budker Institute of Nuclear Physics SB RAS, Novosibirsk 630090, Russia*
[9b]*Novosibirsk State University, Novosibirsk 630090, Russia*
[9c]*Novosibirsk State Technical University, Novosibirsk 630092, Russia*
[10]*University of California at Irvine, Irvine, California 92697, USA*
[11]*University of California at Riverside, Riverside, California 92521, USA*
[12]*University of California at Santa Barbara, Santa Barbara, California 93106, USA*
[13]*University of California at Santa Cruz, Institute for Particle Physics, Santa Cruz, California 95064, USA*
[14]*California Institute of Technology, Pasadena, California 91125, USA*
[15]*University of Cincinnati, Cincinnati, Ohio 45221, USA*
[16]*University of Colorado, Boulder, Colorado 80309, USA*
[17]*Colorado State University, Fort Collins, Colorado 80523, USA*
[18]*Technische Universität Dortmund, Fakultät Physik, D-44221 Dortmund, Germany*
[19]*Laboratoire Leprince-Ringuet, Ecole Polytechnique, CNRS/IN2P3, F-91128 Palaiseau, France*
[20]*University of Edinburgh, Edinburgh EH9 3JZ, United Kingdom*
[21a]*INFN Sezione di Ferrara, I-44122 Ferrara, Italy*
[21b]*Dipartimento di Fisica e Scienze della Terra, Università di Ferrara, I-44122 Ferrara, Italy*
[22]*INFN Laboratori Nazionali di Frascati, I-00044 Frascati, Italy*
[23a]*INFN Sezione di Genova, I-16146 Genova, Italy*
[23b]*Dipartimento di Fisica, Università di Genova, I-16146 Genova, Italy*
[24]*Indian Institute of Technology Guwahati, Guwahati, Assam 781 039, India*
[25]*Harvard University, Cambridge, Massachusetts 02138, USA*
[26]*Universität Heidelberg, Physikalisches Institut, D-69120 Heidelberg, Germany*
[27]*Humboldt-Universität zu Berlin, Institut für Physik, D-12489 Berlin, Germany*
[28]*Imperial College London, London SW7 2AZ, United Kingdom*
[29]*University of Iowa, Iowa City, Iowa 52242, USA*
[30]*Iowa State University, Ames, Iowa 50011-3160, USA*
[31]*Physics Department, Jazan University, Jazan 22822, Kingdom of Saudia Arabia*
[32]*Johns Hopkins University, Baltimore, Maryland 21218, USA*
[33]*Laboratoire de l'Accélérateur Linéaire, IN2P3/CNRS et Université Paris-Sud 11, Centre Scientifique d'Orsay, F-91898 Orsay Cedex, France*
[34]*Lawrence Livermore National Laboratory, Livermore, California 94550, USA*
[35]*University of Liverpool, Liverpool L69 7ZE, United Kingdom*
[36]*Queen Mary, University of London, London E1 4NS, United Kingdom*
[37]*University of London, Royal Holloway and Bedford New College, Egham, Surrey TW20 0EX, United Kingdom*
[38]*University of Louisville, Louisville, Kentucky 40292, USA*
[39]*Johannes Gutenberg-Universität Mainz, Institut für Kernphysik, D-55099 Mainz, Germany*
[40]*University of Manchester, Manchester M13 9PL, United Kingdom*
[41]*University of Maryland, College Park, Maryland 20742, USA*
[42]*Massachusetts Institute of Technology, Laboratory for Nuclear Science, Cambridge, Massachusetts 02139, USA*
[43]*McGill University, Montréal, Québec, Canada H3A 2T8*
[44a]*INFN Sezione di Milano, I-20133 Milano, Italy*
[44b]*Dipartimento di Fisica, Università di Milano, I-20133 Milano, Italy*
[45]*University of Mississippi, University, Mississippi 38677, USA*
[46]*Université de Montréal, Physique des Particules, Montréal, Québec, Canada H3C 3J7*
[47a]*INFN Sezione di Napoli, I-80126 Napoli, Italy*
[47b]*Dipartimento di Scienze Fisiche, Università di Napoli Federico II, I-80126 Napoli, Italy*
[48]*NIKHEF, National Institute for Nuclear Physics and High Energy Physics, NL-1009 DB Amsterdam, The Netherlands*
[49]*University of Notre Dame, Notre Dame, Indiana 46556, USA*
[50]*Ohio State University, Columbus, Ohio 43210, USA*
[51a]*INFN Sezione di Padova, I-35131 Padova, Italy*
[51b]*Dipartimento di Fisica, Università di Padova, I-35131 Padova, Italy*
[52]*Laboratoire de Physique Nucléaire et de Hautes Energies, IN2P3/CNRS, Université Pierre et Marie Curie-Paris6, Université Denis Diderot-Paris7, F-75252 Paris, France*
[53a]*INFN Sezione di Perugia, I-06123 Perugia, Italy*
[53b]*Dipartimento di Fisica, Università di Perugia, I-06123 Perugia, Italy*
[54a]*INFN Sezione di Pisa, I-56127 Pisa, Italy*

[54b]Dipartimento di Fisica, Università di Pisa, I-56127 Pisa, Italy
[54c]Scuola Normale Superiore di Pisa, I-56127 Pisa, Italy
[55]Princeton University, Princeton, New Jersey 08544, USA
[56a]INFN Sezione di Roma, I-00185 Roma, Italy
[56b]Dipartimento di Fisica, Università di Roma La Sapienza, I-00185 Roma, Italy
[57]Universität Rostock, D-18051 Rostock, Germany
[58]Rutherford Appleton Laboratory, Chilton, Didcot, Oxon OX11 0QX, United Kingdom
[59]CEA, Irfu, SPP, Centre de Saclay, F-91191 Gif-sur-Yvette, France
[60]SLAC National Accelerator Laboratory, Stanford, California 94309, USA
[61]University of South Carolina, Columbia, South Carolina 29208, USA
[62]Southern Methodist University, Dallas, Texas 75275, USA
[63]Stanford University, Stanford, California 94305-4060, USA
[64]State University of New York, Albany, New York 12222, USA
[65]Tel Aviv University, School of Physics and Astronomy, Tel Aviv 69978, Israel
[66]University of Tennessee, Knoxville, Tennessee 37996, USA
[67]University of Texas at Austin, Austin, Texas 78712, USA
[68]University of Texas at Dallas, Richardson, Texas 75083, USA
[69a]INFN Sezione di Torino, I-10125 Torino, Italy
[69b]Dipartimento di Fisica, Università di Torino, I-10125 Torino, Italy
[70a]INFN Sezione di Trieste, I-34127 Trieste, Italy
[70b]Dipartimento di Fisica, Università di Trieste, I-34127 Trieste, Italy
[71]IFIC, Universitat de Valencia-CSIC, E-46071 Valencia, Spain
[72]University of Victoria, Victoria, British Columbia, Canada V8W 3P6
[73]Department of Physics, University of Warwick, Coventry CV4 7AL, United Kingdom
[74]University of Wisconsin, Madison, Wisconsin 53706, USA

(Received 27 March 2014; published 16 June 2014)

We study the processes $\gamma\gamma \to K^+K^-\eta$ and $\gamma\gamma \to K^+K^-\pi^0$ using a data sample of 519 fb^{-1} recorded with the *BABAR* detector operating at the SLAC PEP-II asymmetric-energy e^+e^- collider at center-of-mass energies at and near the $\Upsilon(nS)$ $(n = 2, 3, 4)$ resonances. We observe $\eta_c \to K^+K^-\pi^0$ and $\eta_c \to K^+K^-\eta$ decays, measure their relative branching fraction, and perform a Dalitz plot analysis for each decay. We observe the $K_0^*(1430) \to K\eta$ decay and measure its branching fraction relative to the $K\pi$ decay mode to be $\mathcal{R}(K_0^*(1430)) = \frac{\mathcal{B}(K_0^*(1430)\to K\eta)}{\mathcal{B}(K_0^*(1430)\to K\pi)} = 0.092 \pm 0.025^{+0.010}_{-0.025}$. The $\eta_c \to K^+K^-\eta$ and $K_0^*(1430) \to K\eta$ results correspond to the first observations of these channels. The data also show evidence for $\eta_c(2S) \to K^+K^-\pi^0$ and first evidence for $\eta_c(2S) \to K^+K^-\eta$.

DOI: 10.1103/PhysRevD.89.112004 PACS numbers: 13.25.Gv, 14.40.Be, 14.40.Df, 14.40.Pq

I. INTRODUCTION

Charmonium decays, in particular J/ψ radiative and hadronic decays, have been studied extensively [1,2]. One of the motivations for these studies is the search for non-$q\bar{q}$ mesons such as glueballs or molecular states that are predicted by QCD to populate the low mass region of the hadron mass spectrum [3]. Recently, a search for exotic resonances was performed through Dalitz plot analyses of χ_{c1} states [4].

Scalar mesons are still a puzzle in light-meson spectroscopy: there are too many states and they are not consistent with the quark model. In particular, the $f_0(1500)$ resonance, discovered in $\bar{p}p$ annihilations, has been interpreted as a scalar glueball [5]. However, no evidence for the $f_0(1500)$ state has been found in charmonium decays. Another glueball candidate is the $f_0(1710)$ discovered in radiative J/ψ decays. Recently, $f_0(1500)$ and $f_0(1710)$ signals have been incorporated in a Dalitz plot analysis of $B \to 3K$ decays [6]. Charmless $B \to KX$ decays could show enhanced gluonium production [7]. Another puzzling state is the $K_0^*(1430)$ resonance, never observed as a clear peak in the $K\pi$ mass spectrum. In the

*Deceased.
†Present address: the University of Tabuk, Tabuk 71491, Saudi Arabia.
‡Also at Università di Perugia, Dipartimento di Fisica, Perugia, Italy.
§Present address: Laboratoire de Physique Nucléaire et de Hautes Energies, IN2P3/CNRS, Paris, France.
¶Present address: the University of Huddersfield, Huddersfield HD1 3DH, United Kingdom.
**Present address: University of South Alabama, Mobile, Alabama 36688, USA
††Also at Università di Sassari, Sassari, Italy
‡‡Also with INFN Sezione di Roma, Roma, Italy
§§Present address: Universidad Técnica Federico Santa Maria, Valparaiso, Chile 2390123

description of the scalar amplitude in $K\pi$ scattering, the $K_0^*(1430)$ resonance is added coherently to an effective-range description of the low-mass $K\pi$ system in such a way that the net amplitude actually decreases rapidly at the resonance mass. The $K_0^*(1430)$ parameter values were measured by the LASS experiment in the reaction $K^- p \to K^-\pi^+ n$ [8]; the corrected $\mathcal{S}$-wave amplitude representation is given explicitly in Ref. [9]. In the present analysis, we study three-body η_c decays to pseudoscalar mesons and obtain results that are relevant to several issues in light-meson spectroscopy.

Many η_c and $\eta_c(2S)$ decay modes remain unobserved, while others have been studied with very limited statistical precision. In particular, the branching fraction for the decay mode $\eta_c \to K^+K^-\eta$ has been measured by the BESIII experiment based on a fitted yield of only 6.7 ± 3.2 events [10]. No Dalitz plot analysis has been performed on η_c three-body decays.

We describe herein a study of the $K^+K^-\eta$ and $K^+K^-\pi^0$ systems produced in two-photon interactions. Two-photon events in which at least one of the interacting photons is not quasireal are strongly suppressed by the selection criteria described below. This implies that the allowed J^{PC} values of any produced resonances are $0^{\pm+}$, $2^{\pm+}$, 3^{++}, $4^{\pm+}\ldots$ [11]. Angular momentum conservation, parity conservation, and charge conjugation invariance imply that these quantum numbers also apply to the final state except that the $K^+K^-\eta$ and $K^+K^-\pi^0$ states cannot be in a $J^P = 0^+$ state.

This article is organized as follows. In Sec. II, a brief description of the *BABAR* detector is given. Section III is devoted to the event reconstruction and data selection. In Sec. IV, we describe the study of efficiency and resolution, while in Sec. V the mass spectra are presented. Section VI is devoted to the measurement of the branching ratios, while Sec. VII describes the Dalitz plot analyses. In Sec. VIII, we report the measurement of the $K_0^*(1430)$ branching ratio, in Sec. IX we discuss its implications for the pseudoscalar meson mixing angle, and in Sec. X we summarize the results.

II. THE *BABAR* DETECTOR AND DATA SET

The results presented here are based on data collected with the *BABAR* detector at the PEP-II asymmetric-energy e^+e^- collider located at SLAC and correspond to an integrated luminosity of 519 fb^{-1} [12] recorded at center-of-mass energies at and near the $\Upsilon(nS)$ $(n = 2, 3, 4)$ resonances. The *BABAR* detector is described in detail elsewhere [13]. Charged particles are detected, and their momenta are measured, by means of a five-layer, double-sided microstrip detector, and a 40-layer drift chamber, both operating in the 1.5 T magnetic field of a superconducting solenoid. Photons are measured and electrons are identified in a CsI(Tl) crystal electromagnetic calorimeter. Charged-particle identification is provided by the measurement of specific energy loss in the tracking devices, and by an internally reflecting, ring-imaging Cherenkov detector. Muons and K_L^0 mesons are detected in the instrumented flux return of the magnet. Monte Carlo (MC) simulated events [14], with sample sizes more than 10 times larger than the corresponding data samples, are used to evaluate signal efficiency and to determine background features. Two-photon events are simulated using the GamGam MC generator [15].

III. EVENT RECONSTRUCTION AND DATA SELECTION

In this analysis, we select events in which the e^+ and e^- beam particles are scattered at small angles and are undetected in the final state. We study the following reactions

$$\gamma\gamma \to K^+K^-\eta, \quad (\eta \to \gamma\gamma), \tag{1}$$

$$\gamma\gamma \to K^+K^-\eta, \quad (\eta \to \pi^+\pi^-\pi^0), \tag{2}$$

and

$$\gamma\gamma \to K^+K^-\pi^0. \tag{3}$$

For reactions (1) and (3), we consider only events for which the number of well-measured charged-particle tracks with transverse momenta greater than 0.1 GeV/c is exactly equal to two. For reaction (2), we require the number of well-measured charged-particle tracks to be exactly equal to four. The charged-particle tracks are fit to a common vertex with the requirements that they originate from the interaction region and that the χ^2 probability of the vertex fit be greater than 0.1%. We observe prominent η_c signals in all three reactions and improve the signal-to-background ratio using the data, in particular the $c\bar{c}$ η_c resonance. In the optimization procedure, we retain only selection criteria that do not remove significant η_c signal. For the reconstruction of $\pi^0 \to \gamma\gamma$ decays, we require the energy of the less-energetic photon to be greater than 30 MeV for reaction (2) and 50 MeV for reaction (3). For $\eta \to \gamma\gamma$ decay, we require the energy of the less energetic photon to be greater than 100 MeV. Each pair of γ's is kinematically fit to a π^0 or η hypothesis requiring it to emanate from the primary vertex of the event, and with the diphoton mass constrained to the nominal π^0 or η mass, respectively [16]. Due to the presence of soft-photon background, we do not impose a veto on the presence of additional photons in the final state. For reaction (1), we require the presence of exactly one η candidate in each event and discard events having additional π^0's decaying to γ's with energy greater than 70 MeV. For reaction (3), we accept no more than two π^0 candidates in the event.

In reaction (2), the η is reconstructed by combining two oppositely charged tracks identified as pions with each of

the π^0 candidates in the event. The η signal mass region is defined as $541 < m(\pi^+\pi^-\pi^0) < 554$ MeV/c^2. The momentum three-vectors of the final-state pions are combined and the energy of the η candidate is computed using the nominal η mass. According to tests with simulated events, this method improves the $K^+K^-\eta$ mass resolution. We check for possible background from the reaction $\gamma\gamma \to K^+K^-\pi^+\pi^-\pi^0$ [17] using η sideband regions and find it to be consistent with zero. Background arises mainly from random combinations of particles from e^+e^- annihilation, from other two-photon processes, and from events with initial-state photon radiation (ISR). The ISR background is dominated by $J^{PC} = 1^{--}$ resonance production [18]. We discriminate against $K^+K^-\eta$ ($K^+K^-\pi^0$) events produced via ISR by requiring $M^2_{\rm rec} \equiv (p_{e^+e^-} - p_{\rm rec})^2 > 10$ (GeV$^2/c^4$, where $p_{e^+e^-}$ is the four-momentum of the initial state and $p_{\rm rec}$ is the four-momentum of the $K^+K^-\eta$ ($K^+K^-\pi^0$) system. This requirement also removes a large fraction of a residual J/ψ contribution.

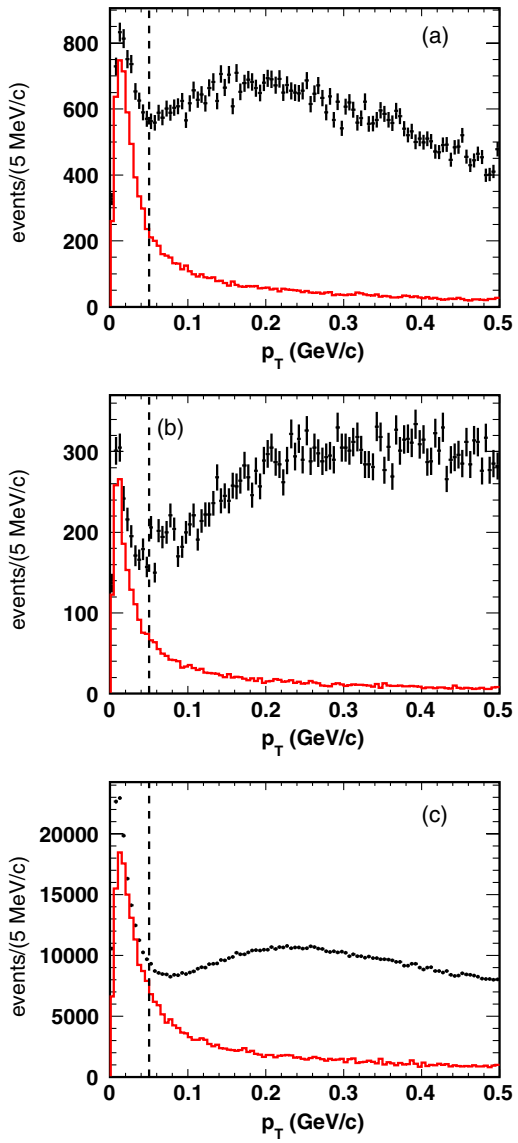

FIG. 1 (color online). Distributions of p_T for (a) $\gamma\gamma \to K^+K^-\eta\,(\eta \to \gamma\gamma)$, (b) $\gamma\gamma \to K^+K^-\eta\,(\eta \to \pi^+\pi^-\pi^0)$, and (c) $\gamma\gamma \to K^+K^-\pi^0$. In each figure the data are shown as points with error bars, and the MC simulation is shown as a histogram; the vertical dashed line indicates the selection applied to isolate two-photon events.

Particle identification is used in two different ways. For reaction (2), with four charged particles in the final state, we require two oppositely charged particles to be loosely identified as kaons and the other two tracks to be consistent with pions. For reactions (1) and (3), with only two charged particles in the final state, we loosely identify one kaon and require that neither track be a well-identified pion, electron, or muon. We define p_T as the magnitude of the vector sum of the transverse momenta, in the e^+e^- rest frame, of the final-state particles with respect to the beam axis. Since well-reconstructed two-photon events are expected to have low values of p_T, we require $p_T < 0.05$ GeV/c. Reaction (3) is affected by background from the reaction $\gamma\gamma \to K^+K^-$ where soft photon background simulates the presence of a low momentum π^0. We reconstruct this mode and reject events having a $\gamma\gamma \to K^+K^-$ candidate with $p_T < 0.1$ GeV/c.

Figure 1 shows the measured p_T distribution for each of the three reactions in comparison to the corresponding p_T distribution obtained from simulation. A peak at low p_T is observed in all three distributions indicating the presence of the two-photon process. The shape of the peak agrees well with that seen in the MC simulation.

IV. EFFICIENCY AND RESOLUTION

To compute the efficiency, η_c and $\eta_c(2S)$ MC signal events for the different channels are generated using a detailed detector simulation [14] in which the η_c and $\eta_c(2S)$ mesons decay uniformly in phase space. These simulated events are reconstructed and analyzed in the same manner as data. The efficiency is computed as the ratio of reconstructed to generated events. Due to the presence of long tails in the Breit-Wigner (BW) representation of the resonances, we apply selection criteria to restrict the generated events to the η_c and $\eta_c(2S)$ mass regions. We express the efficiency as a function of the $m(K^+K^-)$ mass and $\cos\theta$, where θ is the angle in the K^+K^- rest frame between the directions of the K^+ and the boost from the $K^+K^-\eta$ or $K^+K^-\pi^0$ rest frame. To smooth statistical fluctuations, this efficiency is then parametrized as follows.

First we fit the efficiency as a function of $\cos\theta$ in separate intervals of $m(K^+K^-)$, in terms of Legendre polynomials up to $L = 12$:

$$\epsilon(\cos\theta) = \sum_{L=0}^{12} a_L(m) Y_L^0(\cos\theta), \qquad (4)$$

where m denotes K^+K^- invariant mass. For each value of L, we fit the mass dependent coefficients $a_L(m)$ with a seventh-order polynomial in m. Figure 2 shows the resulting fitted efficiency $\epsilon(m, \cos\theta)$ for each of the three reactions. We observe a significant decrease in efficiency for $\cos\theta \sim \pm 1$ and $1.1 < m(K^+K^-) < 1.5$ GeV/c^2 due to the impossibility of reconstructing low-momentum kaons ($p < 200$ MeV/c in the laboratory frame) which have experienced significant energy loss in the beampipe and inner-detector material. The efficiency decrease at high m for $\eta_c \to K^+K^-\eta$ ($\eta \to \pi^+\pi^-\pi^0$) [Fig. 2(b)] results from the loss of a low-momentum π^0 from the η decay.

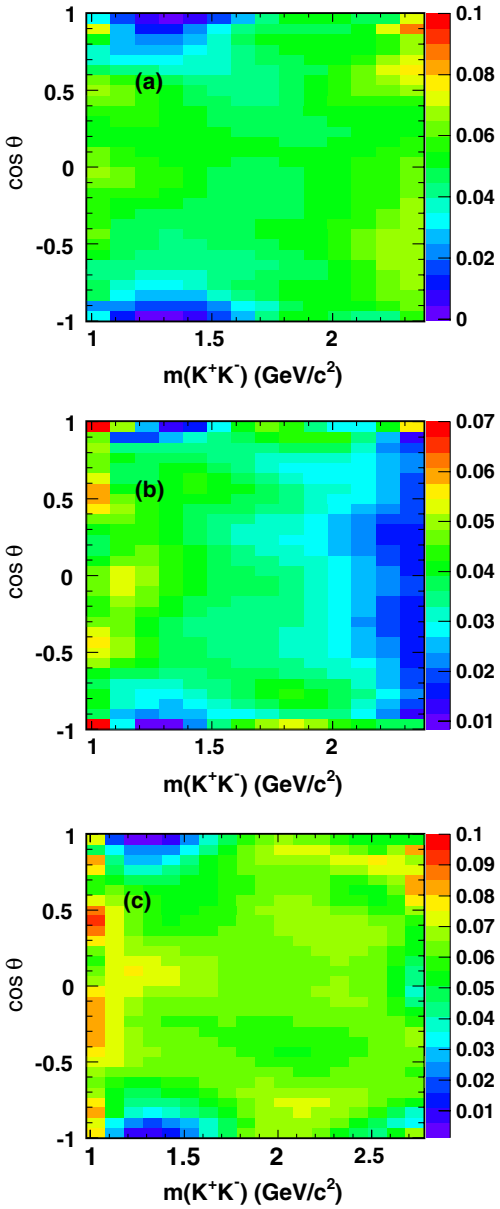

FIG. 2 (color online). Fitted detection efficiency in the $\cos\theta\, vs.\, m(K^+K^-)$ plane for (a) $\eta_c \to K^+K^-\eta$ ($\eta \to \gamma\gamma$), (b) $\eta_c \to K^+K^-\eta$ ($\eta \to \pi^+\pi^-\pi^0$), and (c) $\eta_c \to K^+K^-\pi^0$. Each bin shows the average value of the fit in that region.

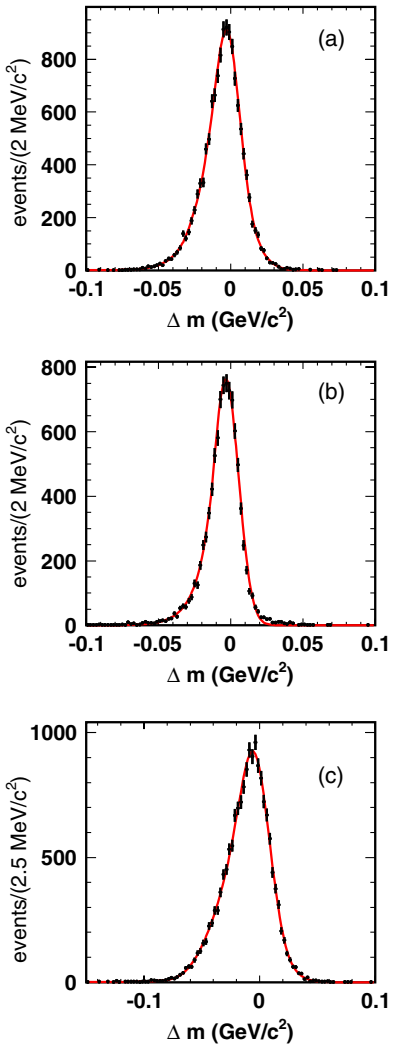

FIG. 3 (color online). MC mass resolution for (a) $\eta_c \to K^+K^-\eta$ ($\eta \to \gamma\gamma$), (b) $\eta_c \to K^+K^-\eta$ ($\eta \to \pi^+\pi^-\pi^0$), and (c) $\eta_c \to K^+K^-\pi^0$. The curves represent the fits described in the text.

The mass resolution, Δm, is measured as the difference between the generated and reconstructed $K^+K^-\eta$ or $K^+K^-\pi^0$ invariant-mass values. Figure 3 shows the Δm distribution for each of the η_c signal regions; these deviate from Gaussian line shapes due to a low-energy tail caused by the response of the CsI calorimeter to photons. We fit the distribution for the $K^+K^-\eta$ ($\eta \to \pi^+\pi^-\pi^0$) final state to a Crystal Ball function [19], and those for the $K^+K^-\eta$ ($\eta \to \gamma\gamma$) and $K^+K^-\pi^0$ final states to a sum of a Crystal Ball function and a Gaussian function. The root-mean-squared values are 15, 14, and 21 MeV/c^2 at the η_c mass, and 18, 15, and 24 MeV/c^2 at the $\eta_c(2S)$ mass, for the $K^+K^-\eta$ ($\eta \to \gamma\gamma$), $K^+K^-\eta$ ($\eta \to \pi^+\pi^-\pi^0$), and $K^+K^-\pi^0$ final states, respectively.

V. MASS SPECTRA

Figure 4(a) shows the $K^+K^-\eta$ mass spectrum, summed over the two η decay modes, before applying the efficiency

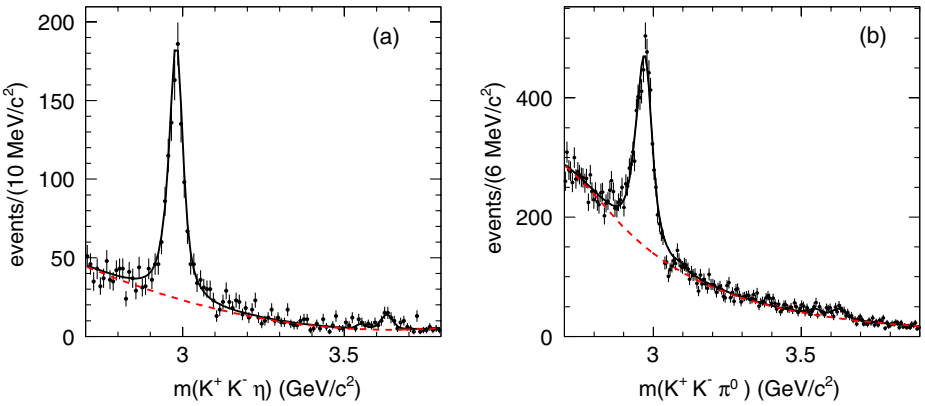

FIG. 4 (color online). (a) The $K^+K^-\eta$ mass spectrum summed over the two η decay modes. (b) The $K^+K^-\pi^0$ mass spectrum. In each figure, the solid curve shows the total fitted function and the dashed curve shows the fitted background contribution.

correction. There are 2950 events in the mass region between 2.7 and 3.8 GeV/c^2, of which 73% are from the $\eta \to \gamma\gamma$ decay mode and 27% are from the $\eta \to \pi^+\pi^-\pi^0$ decay mode. We observe a strong η_c signal and a small enhancement at the position of the $\eta_c(2S)$. The η_c signal-to-background ratio for each of the η decay modes is approximately the same. We perform a simultaneous fit to the $K^+K^-\eta$ mass spectra for the two η decay modes. For each resonance, the mass and width are constrained to take the same fitted values in both distributions. Backgrounds are described by second-order polynomials, and each resonance is represented by a simple Breit-Wigner function convolved with the corresponding resolution function. In addition, we include a signal function for the χ_{c2} resonance with parameters fixed to their PDG values [16]. Figure 4(a) shows the fit result, and Table I summarizes the η_c and $\eta_c(2S)$ parameter values. We have only a weak constraint on the $\eta_c(2S)$ width and so we fix its value to 11.3 MeV [16]. Indicating with ν the number of degrees of freedom, we obtain a good description of the data with $\chi^2/\nu = 194/204$ and a χ^2 probability of 68.1%.

The $K^+K^-\pi^0$ mass spectrum is shown in Fig. 4(b). There are 23 720 events in the mass region between 2.7 and 3.9 GeV/c^2. We observe a strong η_c signal and a small signal at the position of the $\eta_c(2S)$ on top of a sizeable background. We perform a fit to the $K^+K^-\pi^0$ mass spectrum using the background function $B(m) = e^{a_1 m + a_2 m^2}$ for $m < m_0$ and $B(m) = e^{b_0 + b_1 m + b_2 m^2}$ for $m > m_0$, where $m = m(K^+K^-\pi^0)$ and a_i, b_i, and m_0 are free parameters [20]. The two functions and their first derivatives are required to be continuous at m_0, so that the resulting function has only four independent parameters. In addition, we allow for the presence of a residual J/ψ contribution modeled as a simple Gaussian function. Its parameter values are fixed to those from a fit to the $K^+K^-\pi^0$ mass spectrum for the ISR data sample obtained requiring $|M^2_{\rm rec}| < 1$ (GeV/c^2)^2. Figure 4(b) shows the fit to the $K^+K^-\pi^0$ mass spectrum, and Table I summarizes the resulting η_c and $\eta_c(2S)$ parameter values. We obtain a reasonable description of the data with $\chi^2/\nu = 225/189$ and a χ^2 probability of 3.8%.

TABLE I. Fitted η_c and $\eta_c(2S)$ parameter values. The first uncertainty is statistical and the second is systematic.

Resonance	Mass (MeV/c^2)	Γ (MeV)
$\eta_c \to K^+K^-\eta$	$2984.1 \pm 1.1 \pm 2.1$	$34.8 \pm 3.1 \pm 4.0$
$\eta_c \to K^+K^-\pi^0$	$2979.8 \pm 0.8 \pm 3.5$	$25.2 \pm 2.6 \pm 2.4$
$\eta_c(2S) \to K^+K^-\eta$	$3635.1 \pm 5.8 \pm 2.1$	11.3 (fixed)
$\eta_c(2S) \to K^+K^-\pi^0$	$3637.0 \pm 5.7 \pm 3.4$	11.3 (fixed)

The following systematic uncertainties are considered. The background uncertainty contribution is estimated by replacing each function by a third-order polynomial. The mass scale uncertainty is estimated from fits to the J/ψ signal in ISR events. In the case of $\eta_c \to K^+K^-\eta$, we perform independent fits to the mass spectra obtained for the two η decay modes, and consider the mass difference as a measurement of systematic uncertainty. The different contributions are added in quadrature to obtain the values quoted in Table I.

VI. BRANCHING RATIOS

We compute the ratios of the branching fractions for η_c and $\eta_c(2S)$ decays to the $K^+K^-\eta$ final state compared to the respective branching fractions to the $K^+K^-\pi^0$ final state. The ratios are computed as

$$\mathcal{R} = \frac{\mathcal{B}(\eta_c/\eta_c(2S) \to K^+K^-\eta)}{\mathcal{B}(\eta_c/\eta_c(2S) \to K^+K^-\pi^0)} = \frac{N_{K^+K^-\eta}}{N_{K^+K^-\pi^0}} \frac{\epsilon_{K^+K^-\pi^0}}{\epsilon_{K^+K^-\eta}} \frac{1}{\mathcal{B}_\eta}. \quad (5)$$

For each η decay mode, $N_{K^+K^-\eta}$ and $N_{K^+K^-\pi^0}$ represent the fitted yields for η_c and $\eta_c(2S)$ in the $K^+K^-\eta$ and $K^+K^-\pi^0$ mass spectra, $\epsilon_{K^+K^-\eta}$ and $\epsilon_{K^+K^-\pi^0}$ are the corresponding efficiencies, and $\mathcal{B}_\eta$ indicates the particular η branching fraction. The PDG values of the branching fractions are

TABLE II. Summary of the results from the fits to the $K^+K^-\eta$ and $K^+K^-\pi^0$ mass spectra. The table lists event yields, efficiency correction weights, resulting branching ratios and significances. For event yields, the first uncertainty is statistical and the second is systematic. In the evaluation of significances, systematic uncertainties are included.

Channel	Event yield	Weights	$\mathcal{R}$	Significance
$\eta_c \to K^+K^-\pi^0$	$4518 \pm 131 \pm 50$	17.0 ± 0.7		32σ
$\eta_c \to K^+K^-\eta$ $(\eta \to \gamma\gamma)$	$853 \pm 38 \pm 11$	21.3 ± 0.6		21σ
$\mathcal{B}(\eta_c \to K^+K^-\eta)/\mathcal{B}(\eta_c \to K^+K^-\pi^0)$			$0.602 \pm 0.032 \pm 0.065$	
$\eta_c \to K^+K^-\eta$ $(\eta \to \pi^+\pi^-\pi^0)$	$292 \pm 20 \pm 7$	31.2 ± 2.1		14σ
$\mathcal{B}(\eta_c \to K^+K^-\eta)/\mathcal{B}(\eta_c \to K^+K^-\pi^0)$			$0.523 \pm 0.040 \pm 0.083$	
$\eta_c(2S) \to K^+K^-\pi^0$	$178 \pm 29 \pm 39$	14.3 ± 1.3		3.7σ
$\eta_c(2S) \to K^+K^-\eta$	$47 \pm 9 \pm 3$	17.4 ± 0.4		4.9σ
$\mathcal{B}(\eta_c(2S) \to K^+K^-\eta)/\mathcal{B}(\eta_c(2S) \to K^+K^-\pi^0)$			$0.82 \pm 0.21 \pm 0.27$	
$\chi_{c2} \to K^+K^-\pi^0$	$88 \pm 27 \pm 23$			2.5σ
$\chi_{c2} \to K^+K^-\eta$	$2 \pm 5 \pm 2$			0.0σ

$(39.41 \pm 0.20)\%$ and $(22.92 \pm 0.28)\%$ for the $\eta \to \gamma\gamma$ and $\eta \to \pi^+\pi^-\pi^0$, respectively [16].

We estimate the weighted efficiencies $\epsilon_{K^+K^-\eta}$ and $\epsilon_{K^+K^-\pi^0}$ for the η_c signals by making use of the 2-D efficiency functions described in Sec. IV. Due to the presence of non-negligible backgrounds in the η_c signals, which have different distributions in the Dalitz plot, we perform a sideband subtraction by assigning a weight $w = 1/\epsilon(m, \cos\theta)$ to events in the signal region and a negative weight $w = -f/\epsilon(m, \cos\theta)$ to events in the sideband regions. The weight in the sideband regions is scaled down by the factor f to match the fitted η_c signal/background ratio. Therefore we obtain the weighted efficiencies as

$$\epsilon_{K^+K^-\eta/\pi^0} = \frac{\sum_{i=1}^{N} f_i}{\sum_{i=1}^{N} f_i/\epsilon(m_i, \cos\theta_i)}, \tag{6}$$

where N indicates the number of events in the signal +sidebands regions. To remove the dependence of the fit quality on the efficiency functions we make use of the unfitted efficiency distributions. Due to the presence of a sizeable background for the $\eta_c(2S)$, we use the average efficiency value from the simulation.

We determine $N_{K^+K^-\eta}$ and $N_{K^+K^-\pi^0}$ for the η_c by performing fits to the $K^+K^-\eta$ and $K^+K^-\pi^0$ mass spectra. The width is extracted from the simultaneous fit to the $K^+K^-\eta$ mass spectra, and is fixed to this value in the fit to the $K^+K^-\pi^0$ mass spectrum. This procedure is adopted because the signal-to-background ratio at the peak is much better for the $K^+K^-\eta$ mode ($\sim 8:1$ compared to $\sim 2:1$ for the $K^+K^-\pi^0$ mode) while the residual J/ψ contamination is much smaller. The η_c and $\eta_c(2S)$ mass values are determined from the fits. For the $\eta_c(2S)$, we fix the width to 11.3 MeV [16]. The resulting yields, efficiencies, measured branching ratios, and significances are reported in Table II. The significances are evaluated as N_s/σ_T where N_s is the signal event yield and σ_T is the total uncertainty obtained by adding the statistical and systematic contributions in quadrature.

We calculate the weighted mean of the η_c branching-ratio estimates for the two η decay modes and obtain

$$\mathcal{R}(\eta_c) = \frac{\mathcal{B}(\eta_c \to K^+K^-\eta)}{\mathcal{B}(\eta_c \to K^+K^-\pi^0)} = 0.571 \pm 0.025 \pm 0.051, \tag{7}$$

which is consistent with the BESIII measurement of 0.46 ± 0.23 [10]. Since the sample size for $\eta_c(2S) \to K^+K^-\eta$ decays with $\eta \to \pi^+\pi^-\pi^0$ is small, we use only the $\eta \to \gamma\gamma$ decay mode, and obtain

$$\mathcal{R}(\eta_c(2S)) = \frac{\mathcal{B}(\eta_c(2S) \to K^+K^-\eta)}{\mathcal{B}(\eta_c(2S) \to K^+K^-\pi^0)} = 0.82 \pm 0.21 \pm 0.27. \tag{8}$$

In evaluating $\mathcal{R}(\eta_c)$ for the $\eta \to \gamma\gamma$ decay mode, we note that the number of charged-particle tracks and γ's is the same in the numerator and in the denominator of the ratio, so that several systematic uncertainties cancel. Concerning the contribution of the $\eta \to \pi^+\pi^-\pi^0$ decay, we find systematic uncertainties related to the difference in the number of charged-particle tracks to be negligible. We consider the following sources of systematic uncertainty. We modify the η_c width by fixing its value to the PDG value [16]. We modify the background model by using fourth-order polynomials or exponential functions. The uncertainty due to the efficiency weight is evaluated by computing 1000 new weights obtained by randomly modifying the weight in each cell of the $\epsilon(m(K^+K^-), \cos\theta)$ plane according to its statistical uncertainty. The widths of the resulting Gaussian distributions yield the estimate of the systematic uncertainty for the efficiency weighting procedure. These values are reported as the weight uncertainties in Table II.

VII. DALITZ PLOT ANALYSES

We perform Dalitz plot analyses of the $K^+K^-\eta$ and $K^+K^-\pi^0$ systems in the η_c mass region using unbinned

maximum likelihood fits. The likelihood function is written as

$$\mathcal{L} = \prod_{n=1}^{N}\Bigg[f_{\rm sig}(m_n)\cdot\epsilon(x'_n,y'_n)\frac{\sum_{i,j}c_i c_j^* A_i(x_n,y_n)A_j^*(x_n,y_n)}{\sum_{i,j}c_i c_j^* I_{A_i A_j^*}} + (1-f_{\rm sig}(m_n))\frac{\sum_i k_i B_i(x_n,y_n)}{\sum_i k_i I_{B_i}}\Bigg] \quad (9)$$

where

(i) N is the number of events in the signal region;
(ii) for the nth event, m_n is the $K^+K^-\eta$ or the $K^+K^-\pi^0$ invariant mass;
(iii) for the nth event, $x_n = m^2(K^+\eta)$, $y_n = m^2(K^-\eta)$ for $K^+K^-\eta$; $x_n = m^2(K^+\pi^0)$, $y_n = m^2(K^-\pi^0)$ for $K^+K^-\pi^0$;
(iv) $f_{\rm sig}$ is the mass-dependent fraction of signal obtained from the fit to the $K^+K^-\eta$ or $K^+K^-\pi^0$ mass spectrum;
(v) for the nth event, $\epsilon(x'_n,y'_n)$ is the efficiency parametrized as a function $x'_n = m(K^+K^-)$ and $y'_n = \cos\theta$ (see Sec. IV);
(vi) for the nth event, the $A_i(x_n,y_n)$ describe the complex signal-amplitude contributions;
(vii) c_i is the complex amplitude of the ith signal component; the c_i parameters are allowed to vary during the fit process;
(viii) for the nth event, the $B_i(x_n,y_n)$ describe the background probability-density functions assuming that interference between signal and background amplitudes can be ignored;
(ix) k_i is the magnitude of the ith background component; the k_i parameters are obtained by fitting the sideband regions;
(x) $I_{A_iA_j^*} = \int A_i(x,y)A_j^*(x,y)\epsilon(m(K^+K^-),\cos\theta)\,dxdy$ and $I_{B_i} = \int B_i(x,y)dxdy$ are normalization integrals; numerical integration is performed on phase space generated events.

Amplitudes are parametrized as described in Refs. [16] and [21]. The efficiency-corrected fractional contribution f_i due to resonant or nonresonant contribution i is defined as follows:

$$f_i = \frac{|c_i|^2\int|A_i(x,y)|^2dxdy}{\int|\sum_j c_j A_j(x,y)|^2dxdy}. \quad (10)$$

The f_i do not necessarily sum to 100% because of interference effects. The uncertainty for each f_i is evaluated by propagating the full covariance matrix obtained from the fit.

A. Dalitz plot analysis of $\eta_c \to K^+K^-\eta$

We define the η_c signal region as the range 2.922-3.036 GeV/c^2. This region contains 1161 events with $(76.1\pm1.3)\%$ purity, defined as $S/(S+B)$ where S and B indicate the number of signal and background events, respectively, as determined from the fit [Fig. 4(a)]. Sideband regions are defined as the ranges 2.730-2.844 GeV/c^2 and 3.114-3.228 GeV/c^2, respectively. Figure 5 shows the Dalitz plot for the η_c signal region and Fig. 6 shows the Dalitz plot projections.

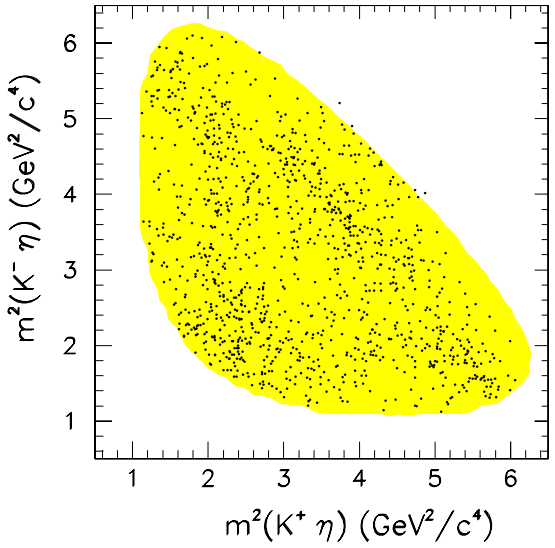

FIG. 5 (color online). Dalitz plot for the $\eta_c \to K^+K^-\eta$ events in the signal region. The shaded area denotes the accessible kinematic region.

We observe signals in the K^+K^- projections corresponding to the $f_0(980)$, $f_0(1500)$, $f_0(1710)$, and $f_0(2200)$ states. We also observe a broad signal in the 1.43 GeV/c^2 mass region in the $K^+\eta$ and $K^-\eta$ projections.

In describing the Dalitz plot, we note that amplitude contributions to the K^+K^- system must have isospin zero in order to satisfy overall isospin conservation in η_c decay. In addition, amplitudes of the form $K^*\bar{K}$ must be symmetrized as $(K^{*+}K^- + K^{*-}K^+)/\sqrt{2}$ so that the decay conserves C-parity. For convenience, these amplitudes are denoted by $K^{*+}K^-$ in the following.

The $f_0(980)$ is parametrized as in a *BABAR* Dalitz plot analysis of $D_s^+ \to K^+K^-\pi^+$ decay [21]. For the $f_0(1430)$ we use the BES parametrization [22]. For the $K_0^*(1430)$, we use our results from the Dalitz plot analysis (see Sec. VII.C), since the individual measurements of the mass and width considered for the PDG average values [16] show a large spread for each parameter. The nonresonant (NR) contribution is parametrized as an amplitude that is constant in magnitude and phase over the Dalitz plot. The $f_0(1500)\eta$ amplitude is taken as the reference amplitude, and so its phase is set to zero. The test of the fit quality is performed by computing a two-dimensional (2-D) χ^2 over the Dalitz plot.

We first perform separate fits to the η_c sidebands using a list of incoherent sum of amplitudes. We find significant contributions from the $f_2'(1525)$, $f_0(2200)$, $K_3^*(1780)$, and $K_0^*(1950)$ resonances, as well as from an incoherent

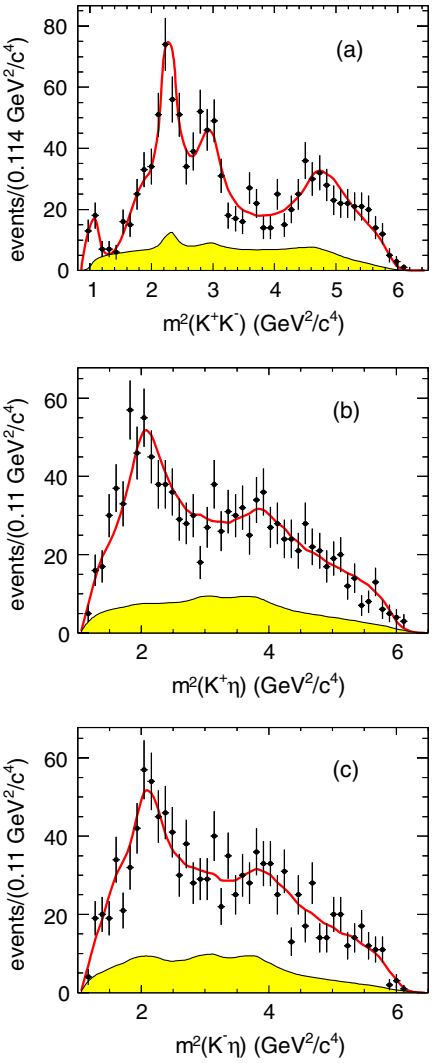

FIG. 6 (color online). The $\eta_c \to K^+K^-\eta$ Dalitz plot projections. The superimposed curves result from the Dalitz plot analysis described in the text. The shaded regions show the background estimates obtained by interpolating the results of the Dalitz plot analyses of the sideband regions.

uniform background. The resulting amplitude fractions are interpolated into the η_c signal region and normalized to yield the fitted purity. Figure 6 shows the projections of the estimated background contributions as shaded distributions.

For the description of the η_c signal, amplitudes are added one by one to ascertain the associated increase of the likelihood value and decrease of the 2-D χ^2. Table III summarizes the fit results for the amplitude fractions and phases. We note that the $f_0(1500)\eta$ amplitude provides the largest contribution. We also observe important contributions from the $K_0^*(1430)^+K^-$, $f_0(980)\eta$, $f_0(2200)\eta$, and $f_0(1710)\eta$ channels. In addition, the fit requires a sizeable *NR* contribution. The sum of the fractions for this η_c decay mode is consistent with 100%.

TABLE III. Results of the Dalitz plot analysis of the $\eta_c \to K^+K^-\eta$ channel.

Final state	Fraction %	Phase (radians)
$f_0(1500)\eta$	$23.7 \pm 7.0 \pm 1.8$	0.
$f_0(1710)\eta$	$8.9 \pm 3.2 \pm 0.4$	$2.2 \pm 0.3 \pm 0.1$
$K_0^*(1430)^+K^-$	$16.4 \pm 4.2 \pm 1.0$	$2.3 \pm 0.2 \pm 0.1$
$f_0(2200)\eta$	$11.2 \pm 2.8 \pm 0.5$	$2.1 \pm 0.3 \pm 0.1$
$K_0^*(1950)^+K^-$	$2.1 \pm 1.3 \pm 0.2$	$-0.2 \pm 0.4 \pm 0.1$
$f_2'(1525)\eta$	$7.3 \pm 3.8 \pm 0.4$	$1.0 \pm 0.1 \pm 0.1$
$f_0(1350)\eta$	$5.0 \pm 3.7 \pm 0.5$	$0.9 \pm 0.2 \pm 0.1$
$f_0(980)\eta$	$10.4 \pm 3.0 \pm 0.5$	$-0.3 \pm 0.3 \pm 0.1$
NR	$15.5 \pm 6.9 \pm 1.0$	$-1.2 \pm 0.4 \pm 0.1$
Sum	$100.0 \pm 11.2 \pm 2.5$	
χ^2/ν	87/65	

We test the statistical significance of the $K_0^*(1430)^+K^-$ contribution by removing it from the list of amplitudes. We obtain a change of the negative log likelihood $\Delta(-2\ln\mathcal{L}) = +107$ and an increase of the χ^2 on the Dalitz plot $\Delta\chi^2 = +76$ for the reduction by 2 parameters. This corresponds to a statistical significance of 10.3 standard deviations. We obtain the first observation of the $K_0^*(1430)^\pm \to K^\pm\eta$ decay mode.

We test the quality of the fit by examining a large sample of MC events at the generator level weighted by the likelihood fitting function and by the efficiency. These events are used to compare the fit result to the Dalitz plot and its projections with proper normalization. The latter comparison is shown in Fig. 6, and good agreement is obtained for all projections. We make use of these weighted events to compute a 2-D χ^2 over the Dalitz plot. For this purpose, we divide the Dalitz plot into a number of cells such that the expected population in each cell is at least eight events. We compute $\chi^2 = \sum_{i=1}^{N_{\rm cells}} (N^i_{\rm obs} - N^i_{\rm exp})^2/N^i_{\rm exp}$, where $N^i_{\rm obs}$ and $N^i_{\rm exp}$ are event yields from data and simulation, respectively. Denoting by $n\,(=16)$ the number of free parameters in the fit, we obtain $\chi^2/\nu = 87/65$ ($\nu = N_{\rm cells} - n$), which indicates that the description of the data is adequate.

We compute the uncorrected Legendre polynomial moments $\langle Y_L^0 \rangle$ in each K^+K^- and $\eta K^\pm$ mass interval by weighting each event by the relevant $Y_L^0(\cos\theta)$ function. These distributions are shown in Figs. 7 and 8. We also compute the expected Legendre polynomial moments from the weighted MC events and compare with the experimental distributions. We observe good agreement for all the distributions, which indicates that the fit is able to reproduce the local structures apparent in the Dalitz plot.

Systematic uncertainty estimates for the fractions and relative phases are computed in two different ways: (i) the purity function is scaled up and down by its statistical uncertainty, and (ii) the parameters of each resonance contributing to the decay are modified within one standard

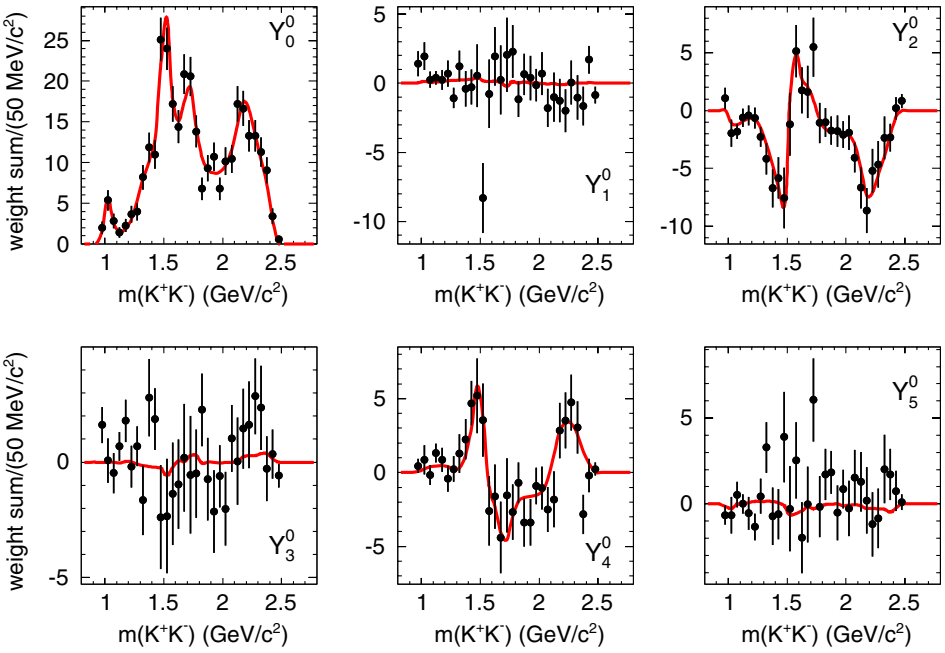

FIG. 7 (color online). Legendre polynomial moments for $\eta_c \to K^+K^-\eta$ as a function of K^+K^- mass. The superimposed curves result from the Dalitz plot analysis described in the text.

deviation of their uncertainties in the PDG average. The two contributions are added in quadrature.

B. Dalitz plot analysis of $\eta_c \to K^+K^-\pi^0$

We define the η_c signal region as the range 2.910-3.030 GeV/c^2, which contains 6710 events with $(55.2 \pm 0.6)\%$ purity. Sideband regions are defined as the ranges 2.720-2.840 GeV/c^2 and 3.100-3.220 GeV/c^2, respectively. Figure 9 shows the Dalitz plot for the η_c signal region, and Fig. 10 shows the corresponding Dalitz plot projections. The Dalitz plot and the mass projections are very similar to the distributions in Ref. [23] for the decay $\eta_c \to K^0_S K^\pm \pi^\mp$.

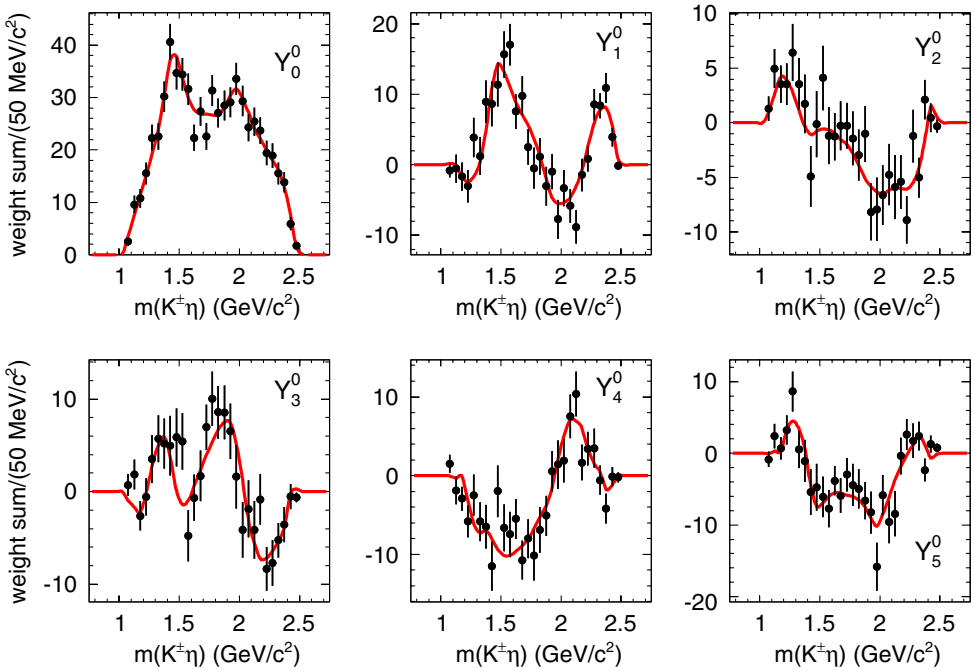

FIG. 8 (color online). Legendre polynomial moments for $\eta_c \to K^+K^-\eta$ as a function of $K^\pm\eta$ mass. The superimposed curves result from the Dalitz plot analysis described in the text. The corresponding $K^+\eta$ and $K^-\eta$ distributions are combined.

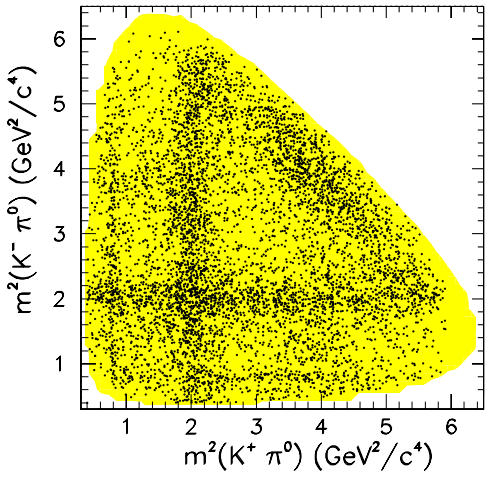

FIG. 9 (color online). Dalitz plot for the events in the $\eta_c \to K^+K^-\pi^0$ signal region. The shaded area denotes the accessible kinematic region.

We observe an enhancement in the low mass region of the K^+K^- mass spectrum due to the presence of the $a_0(980)$, $a_2(1320)$, and $a_0(1450)$ resonances. The $K^\pm\pi^0$ mass spectrum is dominated by the $K_0^*(1430)$ resonance. We also observe $K^*(892)$ signals in the $K^\pm\pi^0$ mass spectrum in both the signal and sideband regions. We fit the η_c sidebands using an incoherent sum of amplitudes, which includes contributions from the $a_2(1320)$, $K^*(892)$, $K_0^*(1430)$, $K_2^*(1430)$, $K^*(1680)$, and $K_0^*(1950)$ resonances and from an incoherent background. As for the Dalitz plot analysis described in Sec. VII.A, the resulting amplitude fractions are interpolated into the η_c signal region and normalized using the results from the fit to the $K^+K^-\pi^0$ mass spectrum. The estimated background contributions are indicated by the shaded regions in Fig. 10.

We perform a Dalitz plot analysis of $\eta_c \to K^+K^-\pi^0$ using a procedure similar to that described for the $\eta_c \to K^+K^-\eta$ analysis in Sec. VII.A. We note that in this case, the amplitude contributions to the K^+K^- system must have isospin one in order to satisfy isospin conservation in η_c decay. As discussed in Sec. VII.A, the $K^*\bar{K}$ amplitudes, again denoted as $K^{*+}K^-$, must be symmetrized in order to conserve C-parity. We take the $K_0^*(1430)^+K^-$ amplitude as the reference, and so set its phase to zero. The $a_0(980)$ resonance is parametrized as a coupled-channel Breit-Wigner resonance whose parameters are taken from Ref. [24]. We do not include an additional $\mathcal{S}$-wave isobar amplitude in the nominal fit. If we include a $K_0^{*+}(800)K^-$ amplitude, as for example in Ref. [25], we find that its contribution is consistent with zero.

Table IV summarizes the amplitude fractions and phases obtained from the fit. Using a method similar to that described in Sec. VII.C, we divide the Dalitz plot into a number of cells such that the number of expected events in each cell is at least eight. In this case there are 12 free parameters and we obtain $\chi^2/\nu = 212/130$. We observe a relatively large χ^2 contribution ($\chi^2 = 19$ for 2 cells) in the lower left corner of the Dalitz plot, where the momentum of the π^0 is very small; this may be due to a residual contamination from $\gamma\gamma \to K^+K^-$ events.

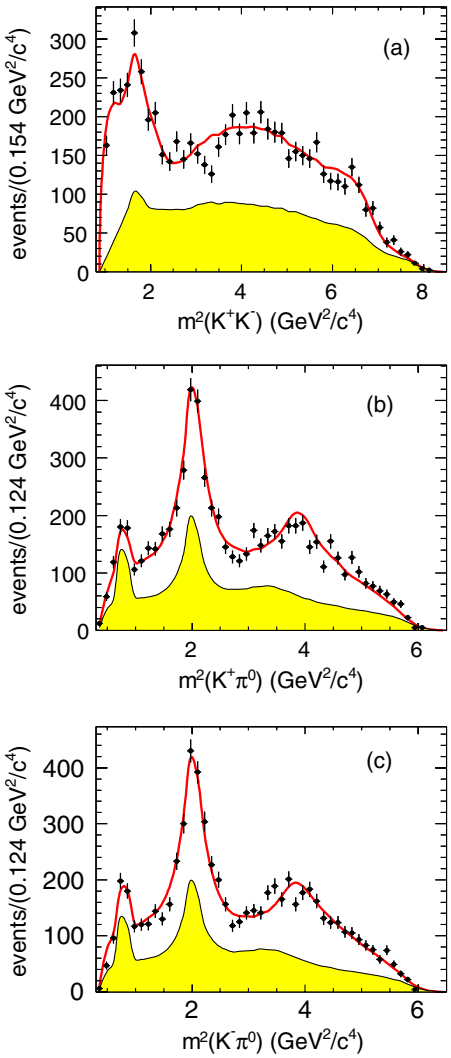

FIG. 10 (color online). The $\eta_c \to K^+K^-\pi^0$ Dalitz plot projections. The superimposed curves result from the Dalitz plot analysis described in the text. The shaded regions show the background estimates obtained by interpolating the results of the Dalitz plot analyses of the sideband regions.

The Dalitz plot analysis shows a dominance of scalar meson amplitudes with small contributions from spin-two resonances. The $K^*(892)$ contribution is consistent with originating entirely from background. Other spin-one K^* resonances have been included in the fit, but their contributions have been found to be consistent with zero. We note the presence of a sizeable nonresonant contribution. However, in this case the sum of the fractions is significantly lower than 100%, indicating important interference effects. Figure 10 shows the fit projections superimposed on the data, and good agreement is apparent for all projections. We compute the uncorrected Legendre

TABLE IV. Results of the Dalitz plot analysis of the $\eta_c \to K^+K^-\pi^0$ channel.

Final state	Fraction %	Phase (radians)
$K_0^*(1430)^+K^-$	$33.8 \pm 1.9 \pm 0.4$	0.
$K_0^*(1950)^+K^-$	$6.7 \pm 1.0 \pm 0.3$	$-0.67 \pm 0.07 \pm 0.03$
$a_0(980)\pi^0$	$1.9 \pm 0.1 \pm 0.2$	$0.38 \pm 0.24 \pm 0.02$
$a_0(1450)\pi^0$	$10.0 \pm 2.4 \pm 0.8$	$-2.4 \pm 0.05 \pm 0.03$
$a_2(1320)\pi^0$	$2.1 \pm 0.1 \pm 0.2$	$0.77 \pm 0.20 \pm 0.04$
$K_2^*(1430)^+K^-$	$6.8 \pm 1.4 \pm 0.3$	$-1.67 \pm 0.07 \pm 0.03$
NR	$24.4 \pm 2.5 \pm 0.6$	$1.49 \pm 0.07 \pm 0.03$
Sum	$85.8 \pm 3.6 \pm 1.2$	
χ^2/ν	212/130	

polynomial moments $\langle Y_L^0 \rangle$ in each K^+K^- and $K^\pm\pi^0$ mass interval by weighting each event by the relevant $Y_L^0(\cos\theta)$ function. These distributions are shown in Figs. 11 and 12. We also compute the expected Legendre polynomial moments from weighted MC events and compare them with the experimental distributions. We observe satisfactory agreement in all distributions, but we note that there are regions in which the detailed behavior of some moments is not well reproduced by the fit. This is reflected by the high value of the χ^2 obtained. We have been unable to find additional amplitudes that improve the fit model. This may indicate, for example, that interference between signal and background is relevant to the Dalitz plot description.

Systematic uncertainty estimates on the fractions and relative phases are obtained by procedures similar to those described in Sec. VII.B.

C. Determination of the $K_0^*(1430)$ parameter values

In the Dalitz plot analyses of $\eta_c \to K^+K^-\eta$ and $\eta_c \to K^+K^-\pi^0$, we perform a likelihood scan to obtain the best-fit parameters for the $K_0^*(1430)$. We use this approach because, in the presence of several interfering scalar-meson resonances, allowing the parameters of the $K_0^*(1430)$ to be free results in fit instabilities. The best measurements of the $K_0^*(1430)$ parameters have been obtained by the LASS experiment [8], in which the mass value $m = 1435 \pm 5$ MeV/c^2 and width value $\Gamma = 279 \pm 6$ MeV were found for the $K_0^*(1430)$ [9]. First, we fix the mass to 1435 MeV/c^2 and examine $-2\ln\mathcal{L}$ as a function of the $K_0^*(1430)$ width. We find that the function has a minimum at 210 MeV for both η_c decay modes. We determine the uncertainty by requiring $\Delta(-2\ln\mathcal{L}) = 1$. We obtain $\Gamma = 210 \pm 20$ MeV and $\Gamma = 240^{+60}_{-50}$ MeV from the $\eta_c \to K^+K^-\pi^0$ and $\eta_c \to K^+K^-\eta$ scans, respectively. Fixing the width to 210 MeV, we then scan the likelihood for the $K_0^*(1430)$ mass and obtain $m = 1438 \pm 8$ MeV/c^2 for the $\eta_c \to K^+K^-\pi^0$ decay mode. Figure 13 shows the results of the likelihood scans. For the $\eta_c \to K^+K^-\eta$ mode, we obtain a minimum at 1435 MeV, but the limited size of the event sample does not permit a useful evaluation of the uncertainty. We evaluate systematic uncertainties for the $K_0^*(1430)$ parameters by repeating the $\eta_c \to K^+K^-\pi^0$ scans for different values of parameters in the ranges of their statistical uncertainties obtaining

$$m(K_0^*(1430)) = 1438 \pm 8 \pm 4 \text{ MeV}/c^2$$
$$\Gamma(K_0^*(1430)) = 210 \pm 20 \pm 12 \text{ MeV}. \quad (11)$$

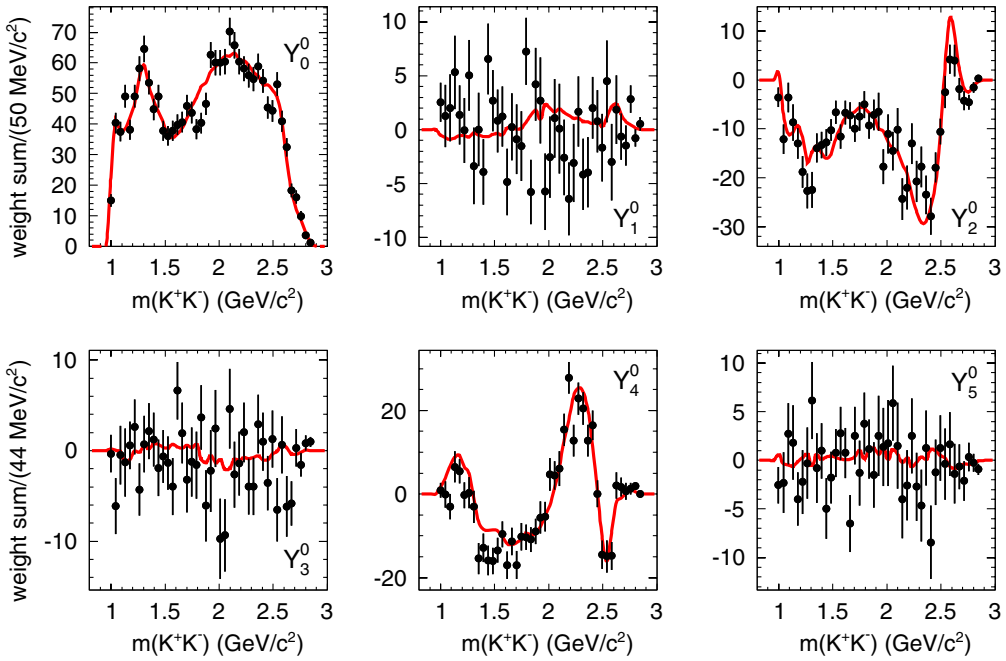

FIG. 11 (color online). Legendre polynomial moments for $\eta_c \to K^+K^-\pi^0$ as a function of K^+K^- mass. The superimposed curves result from the Dalitz plot analysis described in the text.

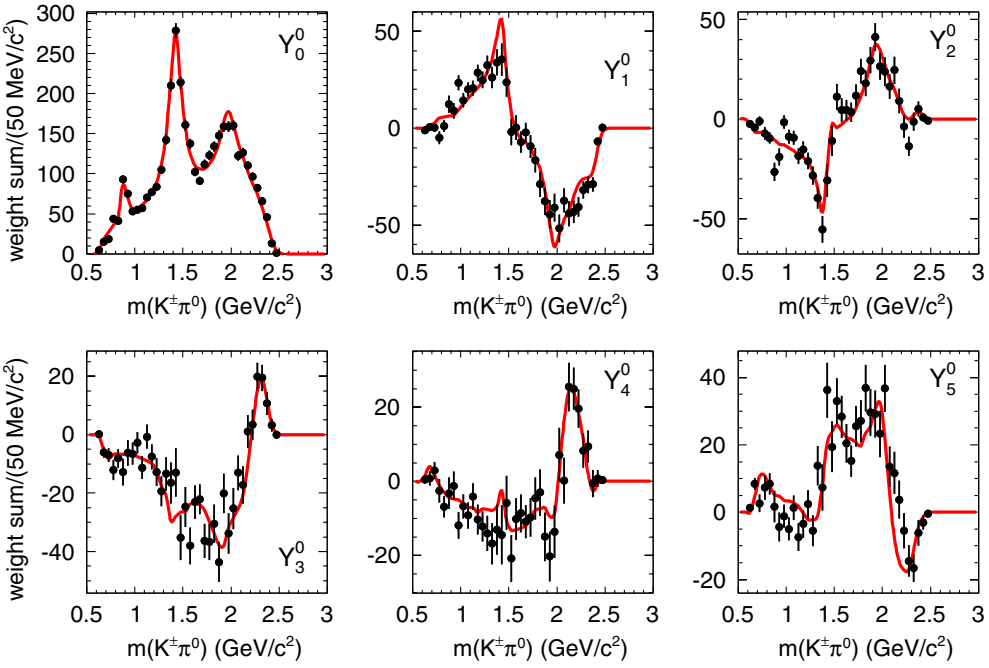

FIG. 12 (color online). Legendre polynomial moments for $\eta_c \to K^+K^-\pi^0$ as a function of $K^\pm\pi^0$ mass. The superimposed curves result from the Dalitz plot analysis described in the text. The corresponding $K^+\pi^0$ and $K^-\pi^0$ distributions are combined.

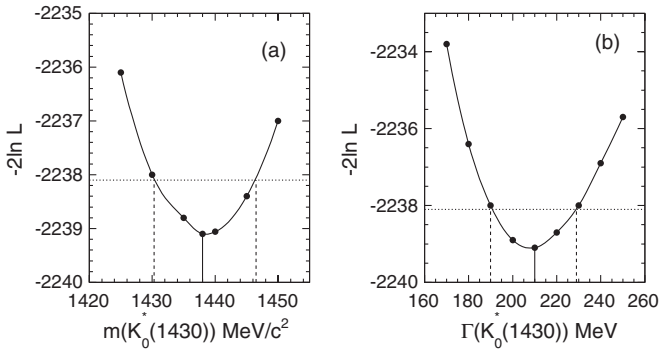

FIG. 13. Likelihood scans as functions of the $K_0^*(1430)$ (a) mass and (b) width. The horizontal (dotted) lines indicate the $\Delta(-2\ln\mathcal{L}) = 1$ positions, the solid line the likelihood minimum, and the vertical (dashed) lines the uncertainty ranges.

The mass value agrees well with that from the LASS experiment, but the width is approximately three standard deviations smaller than the LASS result.

VIII. $K\eta/K\pi$ BRANCHING RATIO FOR THE $K_0^*(1430)$

The observation of the $K_0^*(1430)$ in the $K\eta$ and $K\pi^0$ decay modes permits a measurement of the corresponding branching ratio. Taking into account the systematic uncertainty on the fractions of contributing amplitudes, the Dalitz plot analysis of $\eta_c \to K^+K^-\eta$ decay gives a total $K_0^*(1430)^+K^-$ contribution of

$$f_{\eta K} = 0.164 \pm 0.042 \pm 0.010. \tag{12}$$

Similarly, the Dalitz plot analysis of the $\eta_c \to K^+K^-\pi^0$ decay mode gives a total $K_0^*(1430)^+K^-$ contribution of

$$f_{\pi^0 K} = 0.338 \pm 0.019 \pm 0.004. \tag{13}$$

Using the measurement of $\mathcal{R}(\eta_c)$ from Eq. (6), we obtain the $K_0^*(1430)$ branching ratio

$$\frac{\mathcal{B}(K_0^*(1430) \to \eta K)}{\mathcal{B}(K_0^*(1430) \to \pi K)} = \mathcal{R}(\eta_c)\frac{f_{\eta K}}{f_{\pi K}} = 0.092 \pm 0.025 \pm 0.010, \tag{14}$$

where $f_{\pi K}$ denotes $f_{\pi^0 K}$ after correcting for the $K^0\pi$ decay mode.

We note, however, that in the Dalitz plot analyses the amplitude labeled "*NR*" may be considered to represent an $\mathcal{S}$-wave $K\pi$ or $K\eta$ system in an orbital $\mathcal{S}$-wave state with respect to the bachelor kaon. As such, the *NR* amplitude has structure similar to that of the $K_0^*(1430)^+K^-$ amplitudes, and hence may influence the associated fractional intensity contributions through interference effects. Therefore, we assess an additional systematic uncertainty on the value of the branching ratio given in Eq. (14); this is done in order to account for the impact of the *ad hoc* nature of the representation of the *NR* amplitude.

For example, if we denote the relative phase between the *NR* and $K_0^*(1430)^+K^-$ amplitudes by ϕ_{NR}, the value listed in Table IV is approximately $+\pi/2$, so that the interference term between the amplitudes behaves like the imaginary part of the $K_0^*(1430)$ BW amplitude. This has the same mass dependence as the squared modulus of the BW, and it

follows that the interference term causes the fractional contribution associated with the $K_0^*(1430)^+K^-$ amplitude to be reduced.

We study the correlation between ϕ_{NR} and the $K_0^*(1430)^+K^-$ fraction $f_{\pi^0 K}$ by performing different fits in which ϕ_{NR} is arbitrarily fixed to different values from 0 to $3\pi/2$. We observe a correlation between $f_{\pi^0 K}$ and ϕ_{NR} with $f_{\pi^0 K}$ varying from $(33.3 \pm 1.8)\%$ at $\phi_{NR} = \pi/2$ to $(67.0 \pm 2.2)\%$ at $\phi_{NR} = 3\pi/2$. To estimate the systematic uncertainty related to this effect, we remove the nonresonant contribution in both the $\eta_c \to K^+K^-\eta$ and $\eta_c \to K^+K^-\pi^0$ Dalitz plot analyses. We obtain changes of the negative log likelihood $\Delta(-2\ln\mathcal{L}) = +319$ and $\Delta(-2\ln\mathcal{L}) = +20$ for $\eta_c \to K^+K^-\pi^0$ and $\eta_c \to K^+K^-\eta$ decays, respectively, for the reduction by 2 parameters. The corresponding variation of the $f_{\eta K}/f_{\pi^0 K}$ fraction is -0.023 and we assign this as the associated systematic uncertainty. We thus obtain

$$\frac{\mathcal{B}(K_0^*(1430) \to \eta K)}{\mathcal{B}(K_0^*(1430) \to \pi K)} = \mathcal{R}(\eta_c)\frac{f_{\eta K}}{f_{\pi K}} = 0.092 \pm 0.025^{+0.010}_{-0.025}. \tag{15}$$

The LASS experiment studied the reaction $K^-p \to K^-\eta p$ at 11 GeV/c [26]. The $K^-\eta$ mass spectrum is dominated by the presence of the $K_3^*(1780)$ resonance with no evidence for $K_0^*(1430) \to K\eta$ decay. However, from Ref. [8]

$$\Gamma(K_0^*(1430) \to K\pi)/\Gamma(K_0^*(1430)) = 0.93 \pm 0.04 \pm 0.09, \tag{16}$$

which is not in conflict with the presence of a small branching fraction for the $K\eta$ decay mode.

IX. IMPLICATIONS OF THE $K_0^*(1430)$ BRANCHING RATIO FOR THE PSEUDOSCALAR MESON MIXING ANGLE

As noted in Sec. VIII, there is no evidence for $K_0^*(1430)$ production in the reaction $K^-p \to K^-\eta p$ at 11 GeV/c [26]. There is also no evidence for $K_2^*(1430)$ production in this reaction, and a 0.92% upper limit on the branching ratio $\mathcal{B}(K_2^*(1430) \to K\eta)/\mathcal{B}(K_2^*(1430) \to K\pi)$ is obtained at 95% confidence level. In Ref. [26], this small value is understood in the context of a SU(3) model with octet-singlet mixing of the η and η' [27]. For even angular momentum l (i.e., D-type coupling), it can be shown [28] that a consequence of the resulting $K^*\bar{K}\eta$ couplings is

$$R_l = \frac{\mathcal{B}(K_l^* \to K\eta)}{\mathcal{B}(K_l^* \to K\pi)} = \frac{1}{9}(\cos\theta_p + 2\cdot\sqrt{2}\cdot\sin\theta_p)^2 \cdot (q_{K\eta}/q_{K\pi})^{2l+1} \tag{17}$$

where $q_{K\eta}$ ($q_{K\pi}$) is the kaon momentum in the $K\eta$ ($K\pi$) rest frame at the K^* mass and θ_p is the SU(3) singlet-octet mixing angle for the pseudoscalar meson nonet. We note that R_l equals zero if $\tan\theta_p = -[1/(2\cdot\sqrt{2})]$ (i.e., $\theta_p = -19.7°$).

For $l = 2$, the upper limit $R_2 = 0.0092$ corresponds to $\theta_p = -9.0°$ and the central value yields $\theta_p = -11.4°$.

In the present analysis, we obtain the value $R_0 = 0.092^{+0.027}_{-0.035}$, where we have combined the statistical and systematic uncertainties in quadrature. The corresponding value of θ_p is $(3.1^{+3.3}_{-5.0})°$, which differs by about 2.9 standard deviations from the result obtained from the $K_2^*(1430)$ branching ratio.

The value of R_2 from Ref. [26] is in reasonable agreement with the analysis reported in Ref. [29], which concludes that $\theta_p \sim -20°$ is consistent with experimental evidence from many different sources, although $\theta_p \sim -10°$ cannot be completely ruled out. In addition, a lattice QCD calculation [30] yields $\theta_p = (-14.1 \pm 2.8)°$ for the value of the octet-singlet mixing angle, in good agreement with the spin-two result and the conclusion of Ref. [29], but differing by about three standard deviations from the spin-zero measurement. However, in Ref. [31] it is argued that it is necessary to consider separate octet and singlet mixing angles for the pseudoscalar mesons. For the octet, experimental data from many sources indicate a mixing angle of $\sim -20°$, whereas for the singlet the values are almost entirely in the range from zero to $-10°$. The analysis of Ref. [31] may be able to provide an explanation for the small value of the magnitude of θ_p extracted from our measurement of the $K_0^*(1430)$ branching ratio by using the model suggested in Ref. [27].

X. SUMMARY

We have studied the processes $\gamma\gamma \to K^+K^-\eta$ and $\gamma\gamma \to K^+K^-\pi^0$ using a data sample corresponding to an integrated luminosity of 519 fb^{-1} recorded with the *BABAR* detector at the SLAC PEP-II asymmetric-energy e^+e^- collider at center-of-mass energies at and near the $\Upsilon(nS)$ $(n = 2, 3, 4)$ resonances. We observe $\eta_c \to K^+K^-\pi^0$ decay and obtain the first observation of $\eta_c \to K^+K^-\eta$ decay, measure their relative branching fractions, and perform a Dalitz plot analysis for each decay mode. The Dalitz plot analyses demonstrate the dominance of quasi-two-body amplitudes involving scalar-meson resonances. In particular, we observe significant branching fractions for $\eta_c \to f_0(1500)\eta$ and $\eta_c \to f_0(1710)\eta$. Under the hypothesis of a gluonium content in these resonances, similar decay branching fractions to $\pi\pi$ and $K\bar{K}$ are expected. To obtain these measurements, it would be useful to study $\eta_c \to \eta\pi\pi$, $\eta_c \to \eta' K^+K^-$, and $\eta_c \to \eta'\pi^+\pi^-$ decays. We obtain the first observation of $K_0^*(1430) \to K\eta$ decay, and measure its branching fraction relative to the $K\pi$ mode to be $\mathcal{R}(K_0^*(1430)) = \frac{\mathcal{B}(K_0^*(1430)\to K\eta)}{\mathcal{B}(K_0^*(1430)\to K\pi)} = 0.092 \pm 0.025^{+0.010}_{-0.025}$. This observation is

not in complete agreement with the SU(3) expectation that the $K\eta$ system almost decouples from even-spin K^* resonances [26]. Based on the Dalitz plot analysis of $\eta_c \to K^+K^-\pi^0$, we measure the $K_0^*(1430)$ parameters and obtain $m = 1438 \pm 8 \pm 4$ MeV/c^2 and $\Gamma = 210 \pm 20 \pm 12$ MeV. We observe evidence for $\eta_c(2S) \to K^+K^-\pi^0$ decay, first evidence for $\eta_c(2S) \to K^+K^-\eta$ decay, and measure their relative branching fraction.

ACKNOWLEDGEMENTS

We are grateful for the extraordinary contributions of our PEP-II2 colleagues in achieving the excellent luminosity and machine conditions that have made this work possible. The success of this project also relies critically on the expertise and dedication of the computing organizations that support *BABAR*. The collaborating institutions wish to thank SLAC for its support and the kind hospitality extended to them. This work is supported by the U.S. Department of Energy and National Science Foundation, the Natural Sciences and Engineering Research Council (Canada), the Commissariat à l'Energie Atomique and Institut National de Physique Nucléaire et de Physique des Particules (France), the Bundesministerium für Bildung und Forschung and Deutsche Forschungsgemeinschaft (Germany), the Istituto Nazionale di Fisica Nucleare (Italy), the Foundation for Fundamental Research on Matter (The Netherlands), the Research Council of Norway, the Ministry of Education and Science of the Russian Federation, Ministerio de Economia y Competitividad (Spain), and the Science and Technology Facilities Council (United Kingdom). Individuals have received support from the Marie-Curie IEF program (European Union), the A. P. Sloan Foundation (USA) and the Binational Science Foundation (USA-Israel).

[1] L. Kopke and N. Wermes, Phys. Rep. **174**, 67 (1989).
[2] J. Z. Bai *et al.* (BES Collaboration), Phys. Rev. D **68**, 052003 (2003).
[3] V. Mathieu, N. Kochelev, and V. Vento, Int. J. Mod. Phys. E **18**, 1 (2009).
[4] G. S. Adams *et al.* (CLEO Collaboration), Phys. Rev. D **84**, 112009 (2011).
[5] C. Amsler and F. Close, Phys. Rev. D **53**, 295 (1996).
[6] J. P. Lees *et al.* (*BABAR* Collaboration), Phys. Rev. D **85**, 112010 (2012).
[7] X.-G. He and T. C. Yuan, arXiv:hep-ph/0612108.
[8] D. Aston *et al.* (LASS Collaboration), Nucl. Phys. **B296**, 493 (1988).
[9] B. Aubert *et al.* (*BABAR* Collaboration), Phys. Rev. D **79**, 112001 (2009).
[10] M. Ablikim *et al.* (BESIII Collaboration), Phys. Rev. D **86**, 092009 (2012).
[11] C. N. Yang, Phys. Rev. **77**, 242 (1950).
[12] J. P. Lees *et al.* (*BABAR* Collaboration), Nucl. Instrum. Methods Phys. Res., Sect. A **726**, 203 (2013).
[13] B. Aubert *et al.* (*BABAR* Collaboration), Nucl. Instrum. Methods Phys. Res., Sect. A **479**, 1 (2002); **729**, 615 2013).
[14] The *BABAR* detector Monte Carlo simulation is based on Geant4 [S. Agostinelli *et al.*, Nucl. Instrum. Methods Phys. Res., Sect. A **506**, 250 (2003)] and EvtGen [D. J. Lange, Nucl. Instrum. Methods Phys. Res., Sect. A **462**, 152 (2001)].
[15] B. Aubert *et al.* (*BABAR* Collaboration), Phys. Rev. D **81**, 092003 (2010).
[16] J. Beringer *et al.* (Particle Data Group), Phys. Rev. D **86**, 010001 (2012).
[17] P. del Amo Sanchez *et al.* (*BABAR* Collaboration), Phys. Rev. D **84**, 012004 (2011).
[18] B. Aubert *et al.* (*BABAR* Collaboration), Phys. Rev. D **77**, 092002 (2008).
[19] M. J. Oreglia, Ph.D. thesis, SLAC, Report No. SLAC-R-236, 1980; J. E. Gaiser, Ph.D. thesis, SLAC, Report No. SLAC-R-255, 1982; T. Skwarnicki, Ph.D. thesis, INP and DESY, Report No. DESY-F31-86-02, 1986.
[20] P. del Amo Sanchez *et al.* (*BABAR* Collaboration), Phys. Rev. D **82**, 111101 (2010).
[21] P. del Amo Sanchez *et al.* (*BABAR* Collaboration), Phys. Rev. D **83**, 052001 (2011).
[22] M. Ablikim *et al.* (BES Collaboration), Phys. Lett. B **607**, 243 (2005).
[23] J. P. Lees *et al.* (*BABAR* Collaboration), Phys. Rev. D **81**, 052010 (2010); J. P. Lees *et al.* (*BABAR* Collaboration), Phys. Rev. D **86**, 092005 (2012).
[24] A. Abele *et al.* (Crystal Barrel Collaboration), Phys. Rev. D **57**, 3860 (1998).
[25] E. M. Aitala *et al.* (E791 Collaboration), Phys. Rev. Lett. **89**, 121801 (2002); M. Ablikim *et al.* (BES Collaboration), Phys. Lett. B **633**, 681 (2006).
[26] D. Aston *et al.* (LASS Collaboration), Phys. Lett. B **201**, 169 (1988).
[27] H. J. Lipkin, Phys. Rev. Lett. **46**, 1307 (1981).
[28] H. Hayashi, Ph.D. thesis, Nagoya University, 1988.
[29] F. Gilman and R. Kauffman, Phys. Rev. D **36**, 2761 (1987); **37**, 3348(E) (1988).
[30] N. H. Christ, C. Dawson, T. Izubuchi, C. Jung, Q. Liu, R. D. Mawhinney, C. T. Sachrajda, A. Soni, and R. Zhou (RBC and UKQCD Collaborations), Phys. Rev. Lett. **105**, 241601 (2010).
[31] T. Feldmann, Int. J. Mod. Phys. A **15**, 159 (2000).